

Search for the production of deuterons and antideuterons in e^+e^- annihilation at center-of-mass energies between 4.13 and 4.70 GeV

M. Ablikim *et al.**
(BESIII Collaboration)

 (Received 19 February 2024; accepted 7 May 2024; published 31 May 2024)

Using a data sample of e^+e^- collision data corresponding to an integrated luminosity of 19 fb^{-1} collected with the BESIII detector at the BEPCII collider, we search for the production of deuterons and antideuterons via $e^+e^- \rightarrow pp\pi^-\bar{d} + \text{c.c.}$ for the first time at center-of-mass energies between 4.13 and 4.70 GeV. No significant signal is observed and the upper limit of the $e^+e^- \rightarrow pp\pi^-\bar{d} + \text{c.c.}$ cross section is determined to be from 9.0 to 145 fb depending on the center-of-mass energy at the 90% confidence level.

DOI: [10.1103/PhysRevD.109.092013](https://doi.org/10.1103/PhysRevD.109.092013)

I. INTRODUCTION

In the conventional quark model, mesons are composed of one quark and one antiquark, while baryons are composed of three quarks. However, many states with properties inconsistent with the conventional two or three quark models, such as the $X(3872)$ [1], $Y(4260)$ [2], $Z_c(3900)$ [3,4], $\pi_1(1600)$ [5], and $P_c(4450)$ [6], have been discovered in the last two decades. Numerous theoretical proposals and experimental investigations on the subject of exotic states are reviewed in Refs. [7–11], and there is strong evidence for the existence of tetraquark, pentaquark, and meson-meson and meson-baryon molecular states [7–9].

The study of hadronic states with six quarks, either compact hexaquark states or dibaryon states, has a long history [11–16]. Among them the $d^*(2380)$ has attracted substantial attention [17]. The $d^*(2380)$, with a mass of about 2380 MeV and a width of about 70 MeV, was first observed in the isoscalar double-pionic fusion process $pn \rightarrow d\pi^0\pi^0$ [18], and was later confirmed in other double-pionic fusion processes $pn \rightarrow d\pi^+\pi^-$ [19] and $pp \rightarrow d\pi^+\pi^0$ [20], and non-fusion processes $pn \rightarrow pp\pi^0\pi^-$ [21] and $pn \rightarrow pn\pi^0\pi^0$ [22]. The $d^*(2380)$ has been proposed to be the excited deuteron (d), a molecule with large $\Delta\Delta$ component [23], or a hexaquark state which is dominated by the hidden-color component [24].

The A2 collaboration observed a high spin polarization in the measurement of the recoiling neutron in deuterium photodisintegration, which could be related to the

excitation of the $d^*(2380)$ [25]. Apart from this measurement, most of the results related to the $d^*(2380)$ have so far come from the WASA experiment [18–22], and further studies from other experiments are needed to confirm the existence of the $d^*(2380)$ and to search for other similar states. The production of the antideuteron (\bar{d}) has been studied in several e^+e^- annihilation experiments. The ARGUS [26] and CLEO [27] experiments observed \bar{d} production at the level of 3×10^{-5} per $\Upsilon(1S)$ and $\Upsilon(2S)$ decays, and set limits on production cross section in $\Upsilon(4S)$ decays and $e^+e^- \rightarrow q\bar{q}$ at a center-of-mass energy (\sqrt{s}) of 10.6 GeV. The BABAR [28] experiment performed measurements of inclusive antideuteron production in $\Upsilon(1S)$, $\Upsilon(2S)$, $\Upsilon(3S)$ decays and in e^+e^- annihilation into hadrons at $\sqrt{s} \approx 10.58$ GeV. The ALEPH [29] experiment observed evidence at 3σ significance for \bar{d} production in $e^+e^- \rightarrow q\bar{q}$ at $\sqrt{s} = 91.2$ GeV. Technically, the $d^*(2380)$ state could be studied with these data by combining the detected antideuteron with pions in the same event.

The BESIII experiment [30] collects e^+e^- collision data at \sqrt{s} between 2 and 4.95 GeV. In recent years, the BESIII Collaboration has reported the observation of $e^+e^- \rightarrow 2(p\bar{p})$ [31] and $e^+e^- \rightarrow pp\bar{p}\bar{n}\pi^- + \text{c.c.}$ [32] with the production cross sections on the order of 10 fb. This suggests the production of a deuteron or antideuteron together with two other nucleons may also be observed. In this paper, we search for the production of (anti) deuterons at the BESIII experiment for the first time using the process $e^+e^- \rightarrow pp\pi^-\bar{d} + \text{c.c.}$ at \sqrt{s} from 4.13 to 4.70 GeV.

II. THE BESIII DETECTOR AND DATA SAMPLES

The BESIII detector [30] records symmetric e^+e^- collisions provided by the BEPCII storage ring [33], which operates in the \sqrt{s} range from 2.0 to 4.95 GeV. BESIII has

*Full author list given at the end of the article.

Published by the American Physical Society under the terms of the [Creative Commons Attribution 4.0 International license](https://creativecommons.org/licenses/by/4.0/). Further distribution of this work must maintain attribution to the author(s) and the published article's title, journal citation, and DOI. Funded by SCOAP³.

collected large data samples in this energy region [34]. The cylindrical core of the BESIII detector covers 93% of the full solid angle and consists of a helium-based multilayer drift chamber (MDC), a plastic scintillator time-of-flight system (TOF), and a CsI(Tl) electromagnetic calorimeter (EMC), which are all enclosed in a superconducting solenoidal magnet providing a 1.0 T magnetic field [35]. The solenoid is supported by an octagonal flux-return yoke with resistive plate counter muon identification modules interleaved with steel. The charged-particle momentum resolution at 1 GeV/ c is 0.5%, and the specific energy loss (dE/dx) resolution is 6% for electrons from Bhabha scattering. The EMC measures photon energies with a resolution of 2.5% (5%) at 1 GeV in the barrel (end cap) region. The time resolution in the TOF barrel region is 68 ps, while that in the end cap region is 110 ps. The end cap TOF system was upgraded in 2015 using multi-gap

resistive plate chamber technology, providing a time resolution of 60 ps [36–38].

The data used in this work are listed in Table I. The \sqrt{s} for each dataset was measured using the dimuon process ($e^+e^- \rightarrow \mu^+\mu^-$) with an uncertainty of less than 1.0 MeV [39–41], and the integrated luminosities were measured using the Bhabha process ($e^+e^- \rightarrow e^+e^-$) with an uncertainty of 1.0% [41–43]. The total integrated luminosity of the data used in this work is approximately 19 fb^{-1} , of which about 15 fb^{-1} data samples were collected after the upgrade of the end cap TOF system.

To optimize the selection criteria, determine the detection efficiency and estimate the background contributions, Monte Carlo (MC) simulated samples of events are used. The MC samples are produced with a GEANT4-based [44] software package, which includes the geometric description of the BESIII detector and the detector response. The simulation models the beam energy spread and initial state radiation (ISR) in the e^+e^- annihilations with the generator KKMC [45,46]. The inclusive MC sample includes the production of open charm processes, the ISR production of vector charmoniumlike states, and the continuum processes incorporated in KKMC. The known decay modes of charmonium states are modeled with EVTGEN [47,48] using branching fractions taken from the Particle Data Group [49], and the remaining unknown charmonium decays are modeled with LUNDCHARM [50,51]. Final state radiation from charged final state particles is incorporated using the PHOTOS package [52]. The signal MC samples of the process $e^+e^- \rightarrow pp\pi^-\bar{d}$ together with the charge-conjugate process $e^+e^- \rightarrow \bar{p}\bar{p}\pi^+d$ are generated with a phase space model at each \sqrt{s} .

III. DATA ANALYSIS

To avoid possible bias in the (anti-)deuteron simulation and reconstruction and to improve the selection efficiency, a partial-reconstruction technique is implemented in which only the two protons (antiprotons) and charged π^- (π^+) are reconstructed, and the \bar{d} (d) can be missed. Events with three good charged tracks and with a net charge of one and events with four good charged tracks and with zero net charge are selected as candidates. Hereafter, the charge-conjugate mode is always implied, unless explicitly stated otherwise.

For each good charged track, the polar angle θ is required to be within a range of $|\cos\theta| < 0.93$, where θ is defined with respect to the symmetry axis of the MDC that is taken as the z axis. The distance of closest approach to the interaction point (IP) must be less than 10 cm along the z -axis, $|V_z| < 10$ cm, and less than 1 cm in the transverse plane, $|V_{xy}| < 1$ cm. For particle identification (PID), the specific energy loss dE/dx measured by the MDC and the flight time measured by the TOF are used to form likelihoods $\mathcal{L}(h)$ ($h = p, K, \pi$) for each hadron (h) hypothesis.

TABLE I. The center-of-mass energies (\sqrt{s}), integrated luminosities (\mathcal{L}_{int}), and signal yields for different cases. The uncertainties for signal yields are statistical only.

\sqrt{s} (MeV)	\mathcal{L}_{int} (pb^{-1})	Signal yield			
		Case 1	Case 2	Case 3	Case 4
4128.5	401.5	0.4 ± 1.9	$0.0^{+0.9}$	$0.0^{+0.9}$	$0.0^{+0.9}$
4157.4	408.7	1.0 ± 2.6	$0.0^{+0.9}$	$0.0^{+0.9}$	$0.0^{+0.9}$
4178.0	3189.0	5.7 ± 11.7	$0.0^{+0.9}$	$0.0^{+0.9}$	$0.0^{+0.9}$
4188.8	526.7	4.7 ± 4.4	$0.0^{+0.9}$	$0.0^{+0.9}$	$0.0^{+0.9}$
4198.9	526.0	-0.1 ± 3.6	$0.0^{+0.9}$	$0.0^{+0.9}$	$0.0^{+0.9}$
4209.2	517.1	-1.4 ± 5.1	$0.0^{+0.9}$	$1.0^{+1.4}$	$0.0^{+0.9}$
4218.7	514.6	-2.1 ± 12.6	$0.0^{+0.9}$	$0.0^{+0.9}$	$0.0^{+0.9}$
4226.3	1100.9	-0.7 ± 4.6	$0.0^{+0.9}$	$0.0^{+0.9}$	$0.0^{+0.9}$
4235.7	530.3	3.5 ± 4.4	$0.0^{+0.9}$	$0.0^{+0.9}$	$0.0^{+0.9}$
4243.8	538.1	-2.1 ± 2.2	$0.0^{+0.9}$	$0.0^{+0.9}$	$0.0^{+0.9}$
4258.0	828.4	-2.1 ± 4.5	$0.0^{+0.9}$	$0.0^{+0.9}$	$0.0^{+0.9}$
4266.8	531.1	3.7 ± 4.8	$0.0^{+0.9}$	$0.0^{+0.9}$	$0.0^{+0.9}$
4277.7	175.5	0.0 ± 3.0	$0.0^{+0.9}$	$0.0^{+0.9}$	$0.0^{+0.9}$
4287.9	502.4	-2.1 ± 8.3	$0.0^{+0.9}$	$0.0^{+0.9}$	$0.0^{+0.9}$
4312.0	501.2	0.9 ± 3.4	$0.0^{+0.9}$	$1.0^{+1.4}$	$0.0^{+0.9}$
4337.4	505.0	3.6 ± 3.8	$0.0^{+0.9}$	$0.0^{+0.9}$	$0.0^{+0.9}$
4358.3	543.9	-2.0 ± 7.1	$0.0^{+0.9}$	$0.0^{+0.9}$	$0.0^{+0.9}$
4377.4	522.7	1.8 ± 3.8	$0.0^{+0.9}$	$0.0^{+0.9}$	$0.0^{+0.9}$
4396.4	507.8	-1.8 ± 6.3	$0.0^{+0.9}$	$0.0^{+0.9}$	$0.0^{+0.9}$
4415.6	1090.6	-1.0 ± 3.8	$1.0^{+1.4}_{-0.7}$	$1.0^{+1.4}_{-0.7}$	$0.0^{+0.9}$
4436.2	569.9	6.1 ± 5.1	$0.0^{+0.9}$	$0.0^{+0.9}$	$0.0^{+0.9}$
4467.1	111.1	-2.1 ± 0.6	$0.0^{+0.9}$	$0.0^{+0.9}$	$0.0^{+0.9}$
4527.1	112.1	-2.1 ± 1.6	$0.0^{+0.9}$	$0.0^{+0.9}$	$0.0^{+0.9}$
4599.5	586.9	1.4 ± 4.3	$0.0^{+0.9}$	$0.0^{+0.9}$	$0.0^{+0.9}$
4611.9	103.8	-2.1 ± 1.0	$0.0^{+0.9}$	$0.0^{+0.9}$	$0.0^{+0.9}$
4628.0	521.5	-2.1 ± 1.5	$0.0^{+0.9}$	$0.0^{+0.9}$	$0.0^{+0.9}$
4640.9	552.4	-0.4 ± 3.0	$1.0^{+1.4}_{-0.7}$	$0.0^{+0.9}$	$0.0^{+0.9}$
4661.2	529.6	-2.1 ± 1.4	$0.0^{+0.9}$	$0.0^{+0.9}$	$0.0^{+0.9}$
4681.9	1669.3	-2.1 ± 2.6	$0.0^{+0.9}$	$0.0^{+0.9}$	$0.0^{+0.9}$
4698.8	536.4	3.3 ± 3.5	$0.0^{+0.9}$	$0.0^{+0.9}$	$0.0^{+0.9}$

Tracks are identified as protons when $\mathcal{L}(p) > 0.001$, $\mathcal{L}(p) > \mathcal{L}(K)$ and $\mathcal{L}(p) > \mathcal{L}(\pi)$, while charged pions are identified when $\mathcal{L}(\pi) > 0.001$, $\mathcal{L}(\pi) > \mathcal{L}(p)$ and $\mathcal{L}(\pi) > \mathcal{L}(K)$. To suppress beam-related background contributions, we require the two protons and the π^- to originate from a common vertex and the χ^2 of the vertex fit, χ^2_{VF} , to be less than 70. The vertex position is required to be within a range of $(R_{vx} - 0.12 \text{ cm})^2 + (R_{vy} + 0.14 \text{ cm})^2 \leq (0.5 \text{ cm})^2$ to suppress backgrounds arising from interactions between the beam particles and the beam pipe, where R_{vx} and R_{vy} are the x and y coordinates of the vertex, respectively.

The data samples are divided into four mutually exclusive event classes (cases) that depend on the reconstruction method. For cases 1 and 2, the signal mode is $e^+e^- \rightarrow pp\pi^- \bar{d}$ and the number of reconstructed tracks is 3 or 4, respectively. Similarly, for cases 3 and 4, the signal mode is $e^+e^- \rightarrow \bar{p}\bar{p}\pi^+ d$ and the number of tracks is 3 or 4, respectively. Different selection criteria are applied to events in the four different classes.

For cases 1 and 3, the deuteron track is not reconstructed, either due to the detector coverage or due to the large ionization of the low momentum track. Based on the simulated MC samples, the transverse momentum recoiling against the $pp\pi^-$ system, p_r , is required to be less than $0.35 \text{ GeV}/c$ when $|\cos\theta_r| \leq 0.93$, where θ_r is the opening angle between the recoiling system and the z -axis.

For cases 2 and 4, the deuteron track is reconstructed, and more information can be used to suppress the background. The mass squared of the deuteron candidate calculated using the TOF information, m_d^2 , is required to be within a range of $3.2 < m_d^2 < 4.1 \text{ (GeV}/c^2)^2$. Here, $m_d^2 = p^2 \cdot (\beta^{-2} - 1)/c^2$, and $\beta = L_{\text{path}}/(c \cdot T_{\text{tof}})$, where p is the momentum of the deuteron track, L_{path} is the length of the MDC track extrapolated to the TOF inner radius, T_{tof} is the time of flight corresponding to L_{path} and c is the speed of light. The opening angle θ' between the candidate deuteron track and the recoil direction of the $pp\pi^-$ system, is required to satisfy $\cos\theta' > 0.9$ to suppress background. Studies based on the inclusive MC samples show that the main surviving background is $e^+e^- \rightarrow pp\pi^- \bar{p}\bar{n} + c.c.$ To remove this background process, the number of \bar{p} is required to be zero for case 2 and the number of p is required to be zero for case 4.

IV. BACKGROUND ANALYSIS AND SIGNAL EXTRACTION

After imposing all the requirements mentioned above, the distribution of the recoil mass of the $pp\pi^-$ [$RM(pp\pi^-)$] system in data, inclusive MC, and the weighted signal MC samples summed over all energy points is shown in Fig. 1. For the inclusive MC samples, only a few background events survive, and the remaining events do not form a peak in the

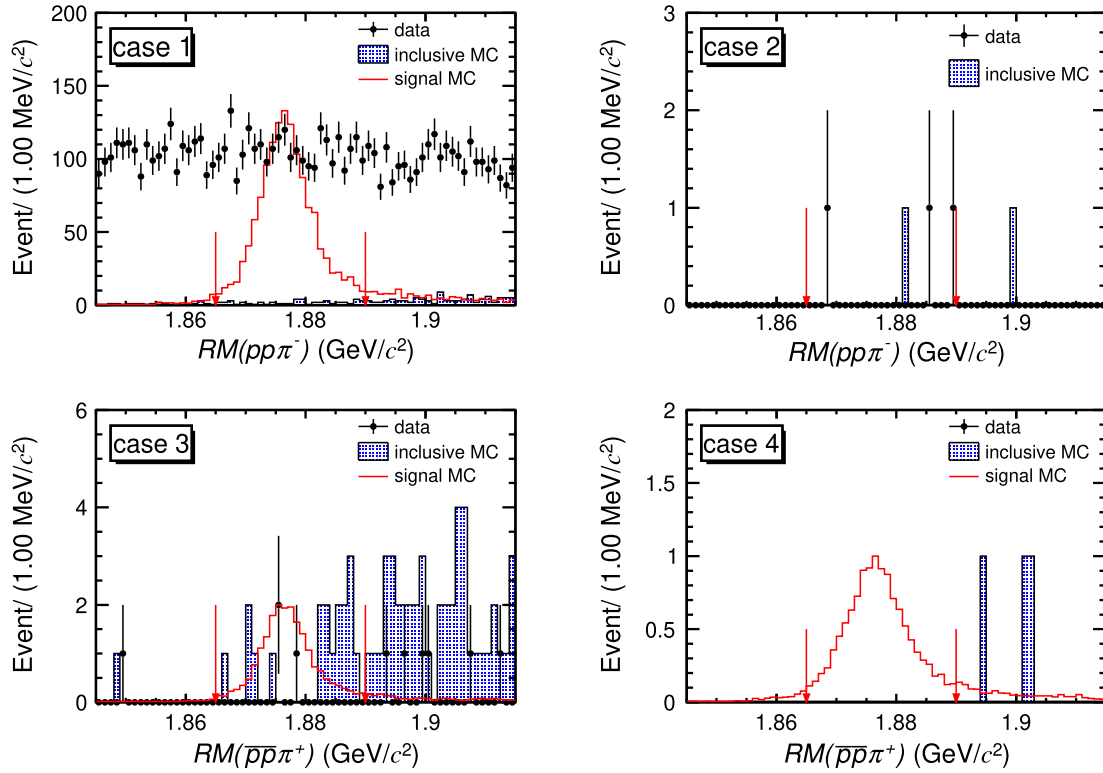


FIG. 1. Distributions of $RM(pp\pi^-)$ and $RM(\bar{p}\bar{p}\pi^+)$ in data (dots with error bars), inclusive MC (shaded histograms) and the weighted signal MC samples (red histograms) summed over all energy points and after all the selections. The \bar{d} cannot be simulated in the current BESIII software system, so there is no signal MC shape in case 2. The region between the two red arrows is the signal region.

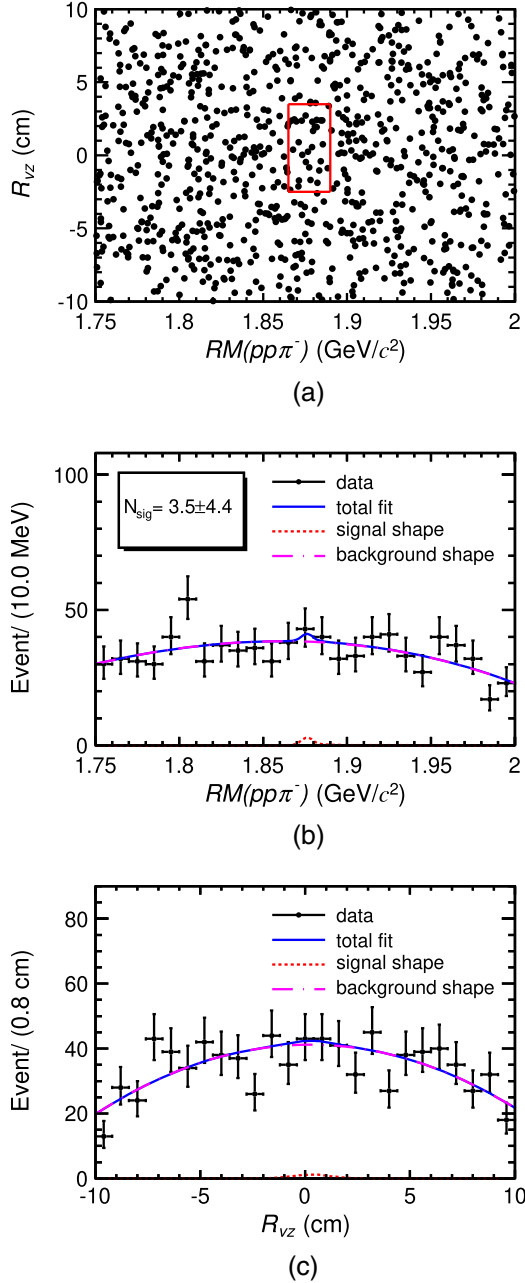


FIG. 2. Two-dimensional distribution for R_{vz} versus $RM(pp\pi^-)$ (a) and the projections of the two-dimensional unbinned fit on $RM(pp\pi^-)$ (b) and R_{vz} (c) in case 1 at $\sqrt{s} = 4235.7 \text{ MeV}$. Here, the red solid box is the signal region, which is used for signal counting in cases 2, 3 and 4. N_{sig} is the signal yield from the fit result.

$RM(pp\pi^-)$ distribution. Only a few events are present in the data samples, except for case 1. The two-dimensional distribution for R_{vz} and $RM(pp\pi^-)$ in case 1 is shown in Fig. 2(a) at $\sqrt{s} = 4235.7 \text{ MeV}$ as an example, where R_{vz} is the z coordinate of the vertex. The smooth R_{vz} distribution in data indicates that the main backgrounds in case 1 are not from e^+e^- annihilation, but from the interaction between beam particles and detector material.

Different methods are used to determine the signal yields in the different cases. For case 1, a two-dimensional unbinned maximum likelihood fit to the $RM(pp\pi^-)$ versus R_{vz} distribution is performed to determine the signal yields. Here, the signal shape is taken from the signal MC samples, and a first or second order polynomial function is used to describe the background shape. Figures 2(b) and 2(c) show the fit result projected on $RM(pp\pi^-)$ and R_{vz} , respectively at $\sqrt{s} = 4235.7 \text{ MeV}$. For the other cases, a ‘‘counting’’ method is used to determine the signal yields. The signal events are selected with both $RM(pp\pi^-)$ and R_{vz} within a window of three standard deviations ($\pm 3\sigma$) around the mean values, i.e., $1.863 < RM(pp\pi^-) < 1.892 \text{ GeV}/c^2$ and $-2.5 < R_{vz} < 3.5 \text{ cm}$, referred to as the signal region. Here the mean values and standard deviations of the $RM(pp\pi^-)$ and R_{vz} distributions are determined from the signal MC samples. The statistical uncertainty of the number of signal events is estimated with the TROLKE [53,54] package in the ROOT [55] framework.

No significant signal is observed from the fit result for case 1, and almost no events survive in the signal region for cases 2, 3 and 4. The signal yields for the different cases are summarized in Table I.

V. DETECTION EFFICIENCY

The signal MC samples are used to determine the detection efficiency. In the GEANT4 software used by the BESIII experiment, the \bar{d} is not simulated. Thus, for cases 1 and 2, which have a \bar{d} in the final state, the detection efficiencies for some of the selection criteria are estimated with control samples selected from data. For cases 3 and 4, the processes can be simulated well and the selection efficiency can be obtained from the signal MC samples directly.

In order to estimate the selection efficiencies for cases 1 and 2, the part of the selection criteria consisting of the requirements on the vertex fit, the vertex position region, and the signal region of $RM(pp\pi^-)$ and R_{vz} are used to select $\bar{p}\bar{p}\pi^+d$ and $pp\pi^-\bar{d}$ processes from the signal MC samples. For each process, the number of tracks can be 3 or 4. Studies based on the high-purity control sample of $e^+e^- \rightarrow p\bar{p}\pi^+\pi^-$ show that the proportions of 3 or 4-track events in $\pi^+\pi^-p$ tagged and $\pi^+\pi^-\bar{p}$ tagged samples are very close. So we assume that the proportion of 3 or 4-track events in the $\bar{p}\bar{p}\pi^+d$ process is also close to that in the $pp\pi^-\bar{d}$ process in this analysis. The difference in the proportions between $\pi^+\pi^-p$ tagged and $\pi^+\pi^-\bar{p}$ tagged samples when the number of tracks equals to 3 or 4 in the control sample is taken as the systematic uncertainty, which will be discussed in detail in the next section. Figure 3(a) shows the efficiencies of the $pp\pi^-\bar{d}$ and $\bar{p}\bar{p}\pi^+d$ processes after the above selection and Fig. 3(b) shows the proportions of 3 and 4-track events in the $\bar{p}\bar{p}\pi^+d$ process. The efficiencies of cases 1 and 2 can be calculated with these numbers accordingly.

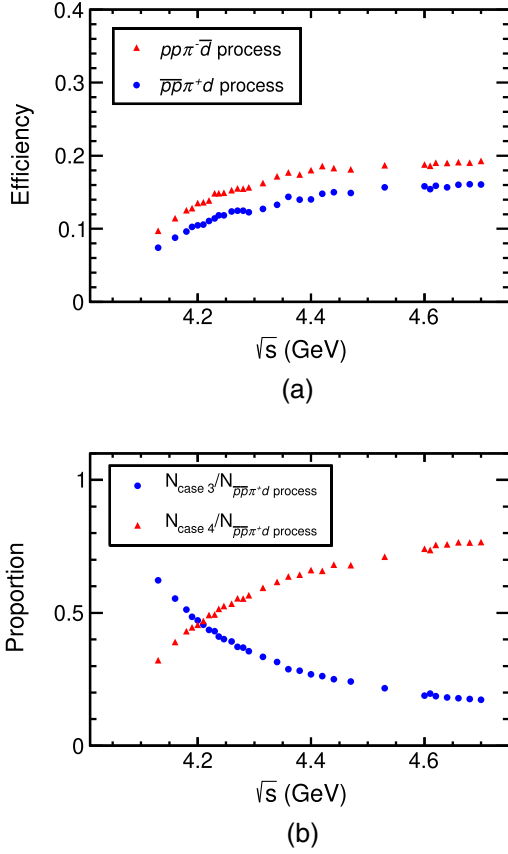


FIG. 3. Efficiencies for the $pp\pi\bar{d}$ (red triangles) and $\bar{p}\bar{p}\pi^+d$ (blue dots) processes after applying part of the selection criteria as described in Sec. V (a), and the proportions of case 3 (blue dots) and 4 (red triangles) events in the $\bar{p}\bar{p}\pi^+d$ process (b).

Table II lists the selection efficiencies for the different event classes. The efficiencies have been corrected for differences between data and MC simulation, as shown by the total correction factors W in this table. The details on the correction factors are discussed in the next section.

VI. SYSTEMATIC UNCERTAINTY

The systematic uncertainties in the cross section measurement originate from the integrated luminosity, the tracking and PID efficiencies, and the determination of the signal yields, which includes the fit range, the signal and background shape, etc. These systematic uncertainties are listed in Table III and discussed in more detail below.

The integrated luminosity is measured using Bhabha scattering events with an uncertainty of 1.0% [41–43].

The tracking and PID efficiencies are studied with a high-purity control sample of $J/\psi \rightarrow p\bar{p}\pi^+\pi^-$ events, and the polar angle and transverse momentum (p_t) dependent efficiencies are measured [56]. The efficiency of MC events is corrected by the two-dimensional efficiency scale factors, and the uncertainty is estimated by varying the efficiency scale factors by one standard deviation for each p_t versus $\cos\theta$ bin. The differences between the new efficiencies and the nominal ones are taken as the systematic uncertainties.

In this analysis, the selection efficiency is corrected according to the measurements with control samples selected from data directly. The efficiency correction factor w^s is defined as

$$w^s = \epsilon_{\text{data}}^s / \epsilon_{\text{MC}}^s, \quad (1)$$

TABLE II. The total correction factor w and the corresponding corrected efficiency ϵ .

\sqrt{s} (MeV)	Case 1		Case 2		Case 3		Case 4	
	W	ϵ	W	ϵ	W	ϵ	W	ϵ
4128.5	0.925	0.056	1.036	0.032	1.023	0.047	1.034	0.025
4157.4	0.925	0.059	1.035	0.046	1.021	0.050	1.031	0.035
4178.0	0.927	0.060	1.035	0.056	1.019	0.050	1.027	0.043
4188.8	0.927	0.058	1.035	0.059	1.018	0.051	1.027	0.047
4198.9	0.927	0.059	1.034	0.064	1.019	0.050	1.025	0.049
4209.2	0.927	0.058	1.033	0.066	1.018	0.049	1.024	0.051
4218.7	0.928	0.056	1.034	0.071	1.018	0.049	1.023	0.056
4226.3	0.929	0.059	1.033	0.076	1.018	0.050	1.022	0.058
4235.7	0.928	0.057	1.034	0.079	1.017	0.049	1.023	0.062
4243.8	0.928	0.056	1.034	0.081	1.017	0.048	1.022	0.064
4258.0	0.929	0.056	1.034	0.084	1.017	0.049	1.022	0.068
4266.8	0.928	0.054	1.032	0.089	1.016	0.047	1.020	0.071
4277.7	0.928	0.053	1.033	0.088	1.016	0.047	1.021	0.070
4287.9	0.929	0.052	1.033	0.092	1.016	0.044	1.020	0.071
4312.0	0.927	0.050	1.033	0.010	1.013	0.043	1.019	0.077
4337.4	0.930	0.050	1.033	0.110	1.015	0.042	1.017	0.083
4358.3	0.931	0.048	1.033	0.116	1.015	0.042	1.017	0.093
4377.4	0.930	0.046	1.033	0.116	1.014	0.040	1.016	0.092

(Table continued)

TABLE II. (*Continued*)

\sqrt{s} (MeV)	Case 1		Case 2		Case 3		Case 4	
	W	ϵ	W	ϵ	W	ϵ	W	ϵ
4396.4	0.930	0.045	1.032	0.123	1.013	0.038	1.015	0.094
4415.6	0.931	0.045	1.032	0.126	1.013	0.039	1.014	0.099
4436.2	0.931	0.043	1.032	0.129	1.013	0.038	1.014	0.104
4467.1	0.932	0.041	1.032	0.127	1.013	0.036	1.013	0.103
4527.1	0.931	0.038	1.032	0.137	1.012	0.034	1.013	0.113
4599.5	0.931	0.032	1.033	0.144	1.010	0.030	1.012	0.118
4611.9	0.931	0.034	1.033	0.142	1.010	0.030	1.012	0.115
4628.0	0.931	0.033	1.032	0.148	1.010	0.030	1.011	0.121
4640.9	0.932	0.032	1.033	0.149	1.010	0.029	1.011	0.120
4661.2	0.931	0.032	1.032	0.151	1.009	0.029	1.011	0.124
4681.9	0.931	0.031	1.032	0.150	1.008	0.028	1.010	0.124
4698.8	0.931	0.031	1.032	0.152	1.009	0.028	1.010	0.124

where the subscripts ‘‘MC’’ and ‘‘data’’ represent MC simulation and data samples, respectively, the superscript ‘‘s’’ represents the selection criterion ‘‘s’’ and ϵ^s is the efficiency for the selection ‘‘s’’ which is calculated as

$$\epsilon^s = \frac{n_{\text{sig}}^s}{n_{\text{sig}}^s + n_{\text{out}}^s}, \quad (2)$$

for both data and MC samples. Here n_{sig}^s is the number of events in the signal region with selection criterion ‘‘s’’ and n_{out}^s is the number of events out of the region of selection criterion ‘‘s’’. The uncertainty of ϵ^s and the uncertainty of w^s is calculated as

$$\sigma_{\epsilon^s} = \frac{n_{\text{out}}^s}{n_{\text{sig}}^s} \cdot \frac{\sqrt{\left(\frac{\sigma_{n_{\text{sig}}^s}}{n_{\text{sig}}^s}\right)^2 + \left(\frac{\sigma_{n_{\text{out}}^s}}{n_{\text{out}}^s}\right)^2}}{\left(1 + \frac{n_{\text{out}}^s}{n_{\text{sig}}^s}\right)^2}, \quad (3)$$

$$\sigma_{w^s} = \frac{\epsilon_{\text{data}}^s}{\epsilon_{\text{MC}}^s} \cdot \sqrt{\left(\frac{\sigma_{\epsilon_{\text{data}}^s}}{\epsilon_{\text{data}}^s}\right)^2 + \left(\frac{\sigma_{\epsilon_{\text{MC}}^s}}{\epsilon_{\text{MC}}^s}\right)^2}, \quad (4)$$

where $\sigma_{n_{\text{sig}}^s}$ and $\sigma_{n_{\text{out}}^s}$ are the uncertainties of n_{sig}^s and n_{out}^s . For $w^s = (1 + \Delta w^s) \pm \sigma_{w^s}$, if $|\frac{\Delta w^s}{\sigma_{w^s}}| < 1.0$, the MC simulation is consistent with the data, no correction will be applied, and $|\Delta w^s| + \sigma_{w^s}$ is taken as the systematic uncertainty. On the other hand, if $|\frac{\Delta w^s}{\sigma_{w^s}}| > 1.0$, the MC efficiency will be corrected to data, and the new efficiency after correction is $\epsilon = \epsilon_{\text{MC}} \cdot w^s$, and σ_{w^s} is taken as the systematic uncertainty. The total correction factor W is defined as $\prod_s w^s$, which is shown in Table II.

The uncertainties of the vertex fit and vertex position are studied using a control sample of $e^+e^- \rightarrow \pi^+\pi^-J/\psi$, $J/\psi \rightarrow e^+e^-/\mu^+\mu^-$ events. The efficiency ratio between data and MC simulation with the vertex fit requirement $\chi_{\text{VF}}^2 < 70$ is $w^{\text{VF}} = 1.002 \pm 0.004$, and we take $\sigma^{\text{VF}} = 0.006$ as the systematic uncertainty and set $w^{\text{VF}} = 1.0$. The efficiency ratio between data and MC simulation with the vertex position requirement $(R_{vx} - 0.12 \text{ cm})^2 + (R_{vy} + 0.14 \text{ cm})^2 \leq (0.5 \text{ cm})^2$ is $w^{\text{VP}} = 1.001 \pm 0.002$, and we take $\sigma^{\text{VP}} = 0.003$ as the systematic uncertainty and set $w^{\text{VP}} = 1.0$.

TABLE III. Relative systematic uncertainties (in units of %) in the cross section measurement of $e^+e^- \rightarrow pp\pi^-\bar{d} + c.c.$

Source	Case 1	Case 2	Case 3	Case 4
Luminosity	1.0	1.0	1.0	1.0
Tracking and PID efficiencies	0.5–1.4	0.7–1.9	0.6–1.5	0.8–1.9
Vertex fit	0.6	0.6	0.6	0.6
R_{vx} and R_{vy}	0.3	0.3	0.3	0.3
p_t and $\cos\theta_r$	2.2–3.1	...	2.2–3.1	...
Opening angle $\cos\theta'$
m_d^2	...	0.6–6.0	...	0.6–6.0
$p(\bar{p})$ veto	...	0.4–2.1	...	0.4–2.1
Efficiency estimation	3.0	1.0
Signal yield extraction	17.7	11.8	11.8	11.8
Total	18.1–18.3	12.0–13.4	12.1–12.3	11.9–13.4

The systematic uncertainty due to the p_t and $\cos\theta_r$ requirements is estimated by loosening or tightening the nominal requirements. The transverse momentum of the track recoiling against the $pp\pi^-$ system, p_t , is required to be less than 0.33 or 0.37 GeV/ c when $|\cos\theta_r| \leq 0.93$. The largest changes of the efficiency compared to the nominal requirement range from 2.2% to 3.1% and are taken as the corresponding uncertainties.

Because we do not have a pure deuteron sample, due to the different time resolution of the TOF between data and MC simulation, the uncertainty from the m_d^2 requirement is studied with the control sample $e^+e^- \rightarrow p\bar{p}\pi^+\pi^-$. The m^2 requirement for the recoil mass of $\pi^+\pi^-\bar{p}$ is applied in the control sample for each \sqrt{s} . Different m^2 ranges are chosen at each energy point to ensure that the efficiency in the control sample is the same as that in this analysis. The efficiency difference between data and MC simulation, which ranges from 0.6% to 6.0%, is taken as the systematic uncertainty.

The systematic uncertainty of the $p(\bar{p})$ veto in the $\bar{p}\bar{p}\pi^+d(pp\pi^-\bar{d})$ process is due to the difference in proportion of deuterons misidentified as protons between data and signal MC samples. The proportion of deuterons misidentified as protons in the simulation can be calculated from the signal MC sample, which is taken as the systematic uncertainty directly since the difference between data and MC sample is small. The corresponding uncertainty ranges from 0.4% to 2.1%.

The efficiency of the $\cos\theta'$ selection is very high due to the loose requirement, and its systematic uncertainty is negligible.

Since the \bar{d} cannot be simulated, the $\bar{p}\bar{p}\pi^+d$ process is used to estimate the efficiency in the $pp\pi^-\bar{d}$ process, which is described in detail in the previous section. To estimate the systematic uncertainty, we take $e^+e^- \rightarrow p\bar{p}\pi^+\pi^-$ as the control sample. The proportions of 3-track or 4-track events in the $\pi^+\pi^-\bar{p}$ tagged and $\pi^+\pi^-p$ tagged samples are obtained from the control sample and the difference in proportions between $\pi^+\pi^-p$ tagged and $\pi^+\pi^-\bar{p}$ tagged samples when the number of tracks equals 3 or 4 is taken as the systematic uncertainty. Based on studies of the control sample, the correction factor and the systematic uncertainty are calculated, where the correction factors are 0.93 and 1.03 for cases 1 and 2, respectively, and the systematic uncertainties are 3% and 1% for cases 1 and 2, respectively.

For the uncertainty of the signal yield extraction, alternative methods are used to estimate the signal yield. For case 1, the uncertainty of the signal yield extraction is estimated by varying the fit range, and changing the signal and background shape. We vary the upper and lower bounds of $RM(pp\pi^-)$ and R_{vz} by ± 5 MeV/ c^2 and ± 1 cm, respectively, use a Gaussian function to describe the signal shape, and use a third-order polynomial function to describe the background shape. The largest difference of the cross section compared with the nominal one is taken as

the systematic uncertainty, which is 17.7%. For cases 2, 3 and 4, the control samples, $e^+e^- \rightarrow p\bar{p}\pi^+\pi^-$ and $J/\psi \rightarrow p\bar{p}\pi^+\pi^-$, are used to estimate the systematic uncertainties of the R_{vz} and $RM(pp\pi^-)$ window selection, respectively. The largest difference in efficiencies between data and simulated MC samples is taken as the systematic uncertainty, which is 11.8%.

The systematic uncertainties for the cross section measurement in different cases are summarized in Table III. The total systematic uncertainty for each case is obtained by summing the individual values in quadrature under the assumption that all the sources are independent.

VII. UPPER LIMIT OF THE CROSS SECTION

The upper limit of the cross section at the 90% confidence level (CL), taking into account the systematic uncertainty, is calculated using a Bayesian method. For case 1, a scan of the likelihood distribution (\mathcal{L}) as a function of the signal yield (N_{sig}) is obtained from fits to $RM(pp\pi^-)$ versus R_{vz} with fixed values for the signal yield. To take the systematic uncertainty into consideration, the likelihood distribution is convolved with a Gaussian function with mean value zero and standard deviation $N_{\text{sig}} \cdot \sigma_{\text{sys}}$. The upper limit on the signal yield ($N_{\text{sig}}^{\text{ul}}$) at the 90% CL is determined as $\int_0^{N_{\text{sig}}^{\text{ul}}} \mathcal{L} dN_{\text{sig}} / \int_0^\infty \mathcal{L} dN_{\text{sig}}$. For cases 2, 3, and 4, a likelihood function is constructed to calculate the signal yield at the 90% CL assuming that the numbers of signal (N_s) and background (N_b) events obey a Poisson distribution, and the efficiency (ϵ) obeys a Gaussian distribution

$$\begin{aligned} P(N_s) &= \text{Pois}(N_s; \epsilon\mu), \\ P(N_b) &= \text{Pois}(N_b; \tau b), \\ P(\epsilon) &= G(\epsilon; z, \sigma_\epsilon), \end{aligned} \quad (5)$$

where μ is the signal rate in the signal region, b is the number of background events in the signal region, z is the efficiency obtained from MC simulation, σ_ϵ is the absolute systematic uncertainty in the efficiency, $\sigma_\epsilon = \epsilon \cdot \sigma_{\text{sys}}$, where σ_{sys} is the relative total systematic uncertainty, and τ is the ratio of the sizes of the sideband regions to the signal regions.

Since there are very few events in the sideband region, we fix b to 0 in the likelihood function to get a more conservative upper limit. The likelihood function is defined as

$$L(\mu, \epsilon | N_s, z) = \frac{(\epsilon\mu)^{N_s}}{N_s!} e^{-\epsilon\mu} \times \frac{1}{\sqrt{2\pi}\sigma_\epsilon} e^{-\frac{(\epsilon-z)^2}{2\sigma_\epsilon^2}}. \quad (6)$$

The upper limit of the signal yield at the 90% CL is determined using Eq. (6). Since the data samples for the four cases are completely independent, the likelihood functions for the different cases can be multiplied to get

TABLE IV. The upper limit of the Born cross section at the 90% CL and the numbers used in the measurement.

\sqrt{s} (MeV)	$1 + \delta$	$\frac{1}{ 1-\Pi ^2}$	$\sigma^{\text{ul}}(pp\pi^-\bar{d})$ (fb)	$\sigma^{\text{ul}}(\bar{p}\bar{p}\pi^+d)$ (fb)	$\sigma^{\text{ul}}(pp\pi^-\bar{d} + \text{c.c.})$ (fb)
4128.5	0.886	1.052	64	43	104
4157.4	0.885	1.053	55	35	88
4178.0	0.897	1.054	6.3	4.1	9.9
4188.8	0.898	1.056	42	23	61
4198.9	0.900	1.056	33	23	55
4209.2	0.903	1.057	31	40	89
4218.7	0.904	1.056	27	22	49
4226.3	0.905	1.056	13	10	23
4235.7	0.908	1.056	28	20	47
4243.8	0.907	1.056	22	20	42
4258.0	0.909	1.054	16	12	28
4266.8	0.912	1.053	27	19	45
4277.7	0.912	1.053	72	58	129
4287.9	0.915	1.053	22	21	43
4312.0	0.917	1.052	23	34	72
4337.4	0.921	1.051	22	19	41
4358.3	0.925	1.051	17	16	33
4377.4	0.925	1.051	20	17	37
4396.4	0.927	1.051	18	17	35
4415.6	0.928	1.052	13	13	36
4436.2	0.932	1.054	17	14	31
4467.1	0.934	1.055	65	75	141
4527.1	0.939	1.054	67	70	137
4599.5	0.896	1.055	14	14	28
4611.9	0.943	1.054	69	76	145
4628.0	0.945	1.054	13	15	29
4640.9	0.946	1.054	23	14	48
4661.2	0.947	1.054	13	14	27
4681.9	0.948	1.054	4.3	4.5	9.0
4698.8	0.949	1.054	14	14	29

a combined likelihood function. The upper limit of the signal yield at the 90% CL for the processes of $e^+e^- \rightarrow pp\pi^-\bar{d}$, $e^+e^- \rightarrow \bar{p}\bar{p}\pi^+d$, and $e^+e^- \rightarrow pp\pi^-\bar{d} + \text{c.c.}$, which with the combination of cases 1 and 2, cases 3 and 4, and all four cases, are calculated. The corresponding upper limit of the Born cross section at the 90% CL is calculated as

$$\sigma^{\text{ul}} = \frac{N_{\text{sig}}^{\text{ul}}}{\mathcal{L} \cdot \epsilon \cdot (1 + \delta) \cdot \frac{1}{|1-\Pi|^2}}, \quad (7)$$

where $N_{\text{sig}}^{\text{ul}}$ is the upper limit of the signal yield at the 90% CL, \mathcal{L} is the integrated luminosity of the dataset, ϵ is the detection efficiency, $(1 + \delta)$ and $\frac{1}{|1-\Pi|^2}$ are the ISR and vacuum polarization [57] correction factors, respectively. We use a flat dressed cross section line shape as the input to generate the signal MC sample and obtain the corresponding ISR correction factor $(1 + \delta)$, since no significant signal is seen in data. The numbers related to the Born cross section measurement are summarized in Table IV. Figure 4 shows the upper limits of the Born cross sections at the 90% CL for the processes of $e^+e^- \rightarrow pp\pi^-\bar{d}$, $e^+e^- \rightarrow \bar{p}\bar{p}\pi^+d$, and $e^+e^- \rightarrow pp\pi^-\bar{d} + \text{c.c.}$ Since no

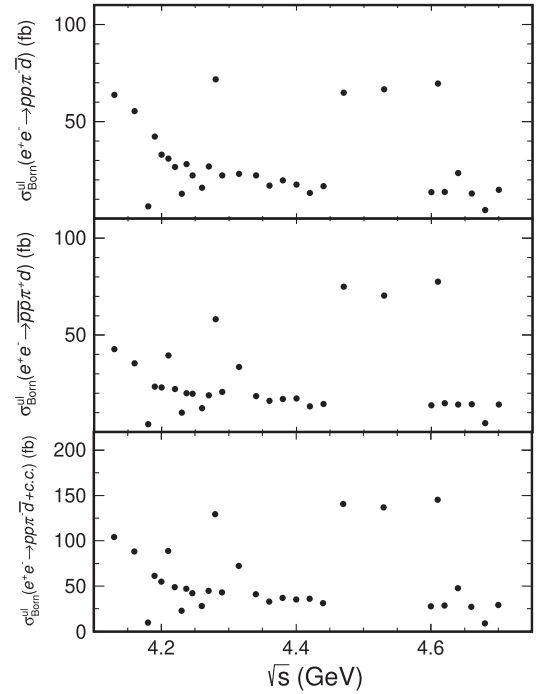


FIG. 4. Upper limits of the Born cross sections at the 90% CL

significant signal was observed, the significant variation in the Born cross section is primarily arises from changes in the luminosity.

VIII. SUMMARY

We search for the process $e^+e^- \rightarrow pp\pi^-\bar{d} + \text{c.c.}$ with the BESIII data at \sqrt{s} from 4.13 to 4.70 GeV. No significant signal is observed. The upper limits at the 90% CL on the Born cross sections of $e^+e^- \rightarrow pp\pi^-\bar{d}$, $\bar{p}\bar{p}\pi^+d$ and $pp\pi^-\bar{d} + \text{c.c.}$ are determined to be from 4.3 to 72 fb, 4.1 to 76 fb, and 9.0 to 145 fb, respectively. The current BESIII sensitivity is in the same order of magnitude as the cross section of inclusive \bar{d} production $\sigma(e^+e^- \rightarrow \bar{d}X) = (9.63 \pm 0.41(\text{stat})_{-1.01}^{+1.17}(\text{syst}))$ fb at $\sqrt{s} \approx 10.58$ GeV from the BABAR experiment [28].

In the BESIII experiment, the low backgrounds guarantee a high sensitivity measurement of the cross section in the process $e^+e^- \rightarrow \bar{p}\bar{p}\pi^+d$ with the number of tracks equal to 3 or 4 and $e^+e^- \rightarrow pp\pi^-\bar{d}$ with the number of tracks equal to 3, and an improved sensitivity may be obtained if the beam backgrounds can be further suppressed in the process $e^+e^- \rightarrow pp\pi^-\bar{d}$ with the number of tracks equal to 4. BEPCII is upgrading the luminosity performance and increasing the maximum \sqrt{s} [34], which will enable a further search for the (anti)deuteron, the $d^*(2380)$, and other possible states with six quarks at the BESIII experiment.

ACKNOWLEDGMENTS

The BESIII collaboration thanks the staff of BEPCII and the IHEP computing center for their strong support. This work is supported in part by National Key R&D Program of China under Contracts No. 2020YFA0406300, No. 2020YFA0406400; National Natural Science Foundation of China (NSFC) under Contracts No. 11635010, No. 11735014, No. 11835012, No. 11935015,

No. 11935016, No. 11935018, No. 11961141012, No. 12022510, No. 12025502, No. 12035009, No. 12035013, No. 12061131003, No. 12192260, No. 12192261, No. 12192262, No. 12192263, No. 12192264, No. 12192265; the Chinese Academy of Sciences (CAS) Large-Scale Scientific Facility Program; the CAS Center for Excellence in Particle Physics (CCEPP); Joint Large-Scale Scientific Facility Funds of the NSFC and CAS under Contract No. U1832207; CAS Key Research Program of Frontier Sciences under Contracts Nos. QYZDJ-SSW-SLH003, No. QYZDJ-SSW-SLH040; 100 Talents Program of CAS; The Institute of Nuclear and Particle Physics (INPAC) and Shanghai Key Laboratory for Particle Physics and Cosmology; ERC under Contract No. 758462; European Union's Horizon 2020 research and innovation programme under Marie Skłodowska-Curie Grant Agreement under Contract No. 894790; German Research Foundation DFG under Contracts No. 443159800, No. 455635585, Collaborative Research Center CRC 1044, FOR5327, GRK 2149; Istituto Nazionale di Fisica Nucleare, Italy; Ministry of Development of Turkey under Contract No. DPT2006K-120470; National Research Foundation of Korea under Contract No. NRF-2022R1A2C1092335; National Science and Technology fund; National Science Research and Innovation Fund (NSRF) via the Program Management Unit for Human Resources & Institutional Development, Research and Innovation under Contract No. B16F640076; Polish National Science Centre under Contract No. 2019/35/O/ST2/02907; Suranaree University of Technology (SUT), Thailand Science Research and Innovation (TSRI), and National Science Research and Innovation Fund (NSRF) under Contract No. 160355; The Royal Society, UK under Contract No. DH160214; The Swedish Research Council; U.S. Department of Energy under Contract No. DE-FG02-05ER41374.

-
- [1] S. K. Choi *et al.* (Belle Collaboration), *Phys. Rev. Lett.* **91**, 262001 (2003).
 [2] B. Aubert *et al.* (BABAR Collaboration), *Phys. Rev. Lett.* **95**, 142001 (2005).
 [3] M. Ablikim *et al.* (BESIII Collaboration), *Phys. Rev. Lett.* **110**, 252001 (2013).
 [4] Z. Q. Liu *et al.* (Belle Collaboration), *Phys. Rev. Lett.* **110**, 252002 (2013); **111**, 019901 (2013).
 [5] G. S. Adams *et al.* (E852 Collaboration), *Phys. Rev. Lett.* **81**, 5760 (1998).
 [6] R. Aaij *et al.* (LHCb Collaboration), *Phys. Rev. Lett.* **115**, 072001 (2015).
 [7] F. K. Guo, C. Hanhart, U.-G. Meißner, Q. Wang, Q. Zhao, and B.-S. Zou, *Rev. Mod. Phys.* **90**, 015004 (2018).
 [8] Y. R. Liu, H. X. Chen, W. Chen, X. Liu, and S. L. Zhu, *Prog. Part. Nucl. Phys.* **107**, 237 (2019).
 [9] N. Brambilla, S. Eidelman, C. Hanhart, A. Nefediev, C.-P. Shen, C. E. Thomas, A. Vairo, and C.-Z. Yuan, *Phys. Rep.* **873**, 1 (2020).
 [10] E. Klempt and A. Zaitsev, *Phys. Rep.* **454**, 1 (2007).
 [11] R. L. Jaffe, *Phys. Rep.* **409**, 1 (2005).
 [12] M. P. Locher, M. E. Sainio, and A. Svarc, *Adv. Nucl. Phys.* **17**, 47 (1986), <https://www.osti.gov/biblio/5235240>.
 [13] M. Abud, F. Buccella, and F. Tramontano, *Phys. Rev. D* **81**, 074018 (2010).
 [14] M. Bashkanov, S. J. Brodsky, and H. Clement, *Phys. Lett. B* **727**, 438 (2013).
 [15] H. Clement, *Prog. Part. Nucl. Phys.* **93**, 195 (2017).

- [16] A. Gal, *Acta Phys. Pol. B* **47**, 471 (2016).
- [17] Y. Dong, P. Shen, and Z. Zhang, *Prog. Part. Nucl. Phys.* **131**, 104045 (2023).
- [18] M. Bashkanov *et al.* (CELSIUS/WASA Collaboration), *Phys. Rev. Lett.* **102**, 052301 (2009).
- [19] P. Adlarson *et al.* (WASA-at-COSY Collaboration), *Phys. Rev. Lett.* **106**, 242302 (2011).
- [20] F. Kren *et al.* (CELSIUS/WASA Collaboration), *Phys. Lett. B* **684**, 110 (2010); **702**, 312 (2011).
- [21] P. Adlarson *et al.* (WASA-at-COSY Collaboration), *Phys. Rev. C* **88**, 055208 (2013).
- [22] P. Adlarson *et al.* (WASA-at-COSY Collaboration), *Phys. Lett. B* **743**, 325 (2015).
- [23] H. X. Huang, J. L. Ping, and F. Wang, *Phys. Rev. C* **89**, 034001 (2014).
- [24] H. Kim, K. S. Kim, and M. Oka, *Phys. Rev. D* **102**, 074023 (2020).
- [25] M. Bashkanov *et al.* (A2 Collaboration), *Phys. Rev. Lett.* **124**, 132001 (2020).
- [26] H. Albrecht *et al.* (ARGUS Collaboration), *Phys. Lett. B* **236**, 102 (1990).
- [27] D. M. Asner *et al.* (CLEO Collaboration), *Phys. Rev. D* **75**, 012009 (2007).
- [28] J. P. Lees *et al.* (BABAR Collaboration), *Phys. Rev. D* **89**, 111102 (2014).
- [29] S. Schael *et al.* (ALEPH Collaboration), *Phys. Lett. B* **639**, 192 (2006).
- [30] M. Ablikim *et al.* (BESIII Collaboration), *Nucl. Instrum. Methods Phys. Res., Sect. A* **614**, 345 (2010).
- [31] M. Ablikim *et al.* (BESIII Collaboration), *Phys. Rev. D* **103**, 052003 (2021).
- [32] M. Ablikim *et al.* (BESIII Collaboration), *Chin. Phys. C* **47**, 043001 (2023).
- [33] C. h. Yu *et al.*, in *7th International Particle Accelerator Conference* (JACoW, Geneva, Switzerland, 2016), p. TUYA01.
- [34] M. Ablikim *et al.* (BESIII Collaboration), *Chin. Phys. C* **44**, 040001 (2020).
- [35] K. X. Huang, Z. J. Li, Z. Qian, J. Zhu, H. Y. Li, Y. M. Zhang, S. S. Sun, and Z. Y. You, *Nucl. Sci. Tech.* **33**, 142 (2022).
- [36] X. Li *et al.*, *Radiat. Detect. Technol. Methods* **1**, 13 (2017).
- [37] Y. X. Guo *et al.*, *Radiat. Detect. Technol. Methods* **1**, 15 (2017).
- [38] P. Cao *et al.*, *Nucl. Instrum. Methods Phys. Res., Sect. A* **953**, 163053 (2020).
- [39] M. Ablikim *et al.* (BESIII Collaboration), *Chin. Phys. C* **40**, 063001 (2016).
- [40] M. Ablikim *et al.* (BESIII Collaboration), *Chin. Phys. C* **45**, 103001 (2021).
- [41] M. Ablikim *et al.* (BESIII Collaboration), *Chin. Phys. C* **46**, 113003 (2022).
- [42] M. Ablikim *et al.* (BESIII Collaboration), *Chin. Phys. C* **46**, 113002 (2022).
- [43] M. Ablikim *et al.* (BESIII Collaboration), *Chin. Phys. C* **39**, 093001 (2015).
- [44] S. Agostinelli *et al.* (GEANT4 Collaboration), *Nucl. Instrum. Methods Phys. Res., Sect. A* **506**, 250 (2003).
- [45] S. Jadach, B. F. L. Ward, and Z. Was, *Phys. Rev. D* **63**, 113009 (2001).
- [46] S. Jadach, B. F. L. Ward, and Z. Was, *Comput. Phys. Commun.* **130**, 260 (2000).
- [47] D. J. Lange, *Nucl. Instrum. Methods Phys. Res., Sect. A* **462**, 152 (2001).
- [48] R. G. Ping, *Chin. Phys. C* **32**, 599 (2008).
- [49] R. L. Workman *et al.* (Particle Data Group), *Prog. Theor. Exp. Phys.* **2022**, 083C01 (2022).
- [50] J. C. Chen, G. S. Huang, X. R. Qi, D. H. Zhang, and Y. S. Zhu, *Phys. Rev. D* **62**, 034003 (2000).
- [51] R. L. Yang, R. G. Ping, and H. Chen, *Chin. Phys. Lett.* **31**, 061301 (2014).
- [52] E. Richter Was, *Phys. Lett. B* **303**, 163 (1993).
- [53] W. A. Rolke, A. M. Lopez, and J. Conrad, *Nucl. Instrum. Methods Phys. Res., Sect. A* **551**, 493 (2005).
- [54] J. Lundberg, J. Conrad, W. Rolke, and A. Lopez, *Comput. Phys. Commun.* **181**, 683 (2010).
- [55] R. Brun and F. Rademakers, *Nucl. Instrum. Methods Phys. Res., Sect. A* **389**, 81 (1997).
- [56] M. Ablikim *et al.* (BESIII Collaboration), *Phys. Rev. Lett.* **126**, 092002 (2021).
- [57] F. Jegerlehner, *Nuovo Cimento Soc. Ital. Fis.* **034S1C**, 31 (2011).

M. Ablikim,¹ M. N. Achasov,^{13,b} P. Adlarson,⁷³ R. Aliberti,³⁴ A. Amoroso,^{72a,72c} M. R. An,³⁸ Q. An,^{69,56} Y. Bai,⁵⁵ O. Bakina,³⁵ I. Balossino,^{29a} Y. Ban,^{45,g} V. Batozskaya,^{1,43} K. Begzsuren,³¹ N. Berger,³⁴ M. Bertani,^{28a} D. Bettoni,^{29a} F. Bianchi,^{72a,72c} E. Bianco,^{72a,72c} J. Bloms,⁶⁶ A. Bortone,^{72a,72c} I. Boyko,³⁵ R. A. Briere,⁵ A. Brueggemann,⁶⁶ H. Cai,⁷⁴ X. Cai,^{1,56} A. Calcaterra,^{28a} G. F. Cao,^{1,61} N. Cao,^{1,61} S. A. Cetin,^{60a} J. F. Chang,^{1,56} T. T. Chang,⁷⁵ W. L. Chang,^{1,61} G. R. Che,⁴² G. Chelkov,^{35,a} C. Chen,⁴² Chao Chen,⁵³ G. Chen,¹ H. S. Chen,^{1,61} M. L. Chen,^{1,56,61} S. J. Chen,⁴¹ S. M. Chen,⁵⁹ T. Chen,^{1,61} X. R. Chen,^{30,61} X. T. Chen,^{1,61} Y. B. Chen,^{1,56} Y. Q. Chen,³³ Z. J. Chen,^{25,h} W. S. Cheng,^{72c} S. K. Choi,¹⁰ X. Chu,⁴² G. Cibinetto,^{29a} S. C. Coen,⁴ F. Cossio,^{72c} J. J. Cui,⁴⁸ H. L. Dai,^{1,56} J. P. Dai,⁷⁷ A. Dbeyssi,¹⁹ R. E. de Boer,⁴ D. Dedovich,³⁵ Z. Y. Deng,¹ A. Denig,³⁴ I. Denysenko,³⁵ M. Destefanis,^{72a,72c} F. De Mori,^{72a,72c} B. Ding,^{64,1} Y. Ding,³³ Y. Ding,³⁹ J. Dong,^{1,56} L. Y. Dong,^{1,61} M. Y. Dong,^{1,56,61} X. Dong,⁷⁴ S. X. Du,⁷⁹ Z. H. Duan,⁴¹ P. Egorov,^{35,a} Y. L. Fan,⁷⁴ J. Fang,^{1,56} S. S. Fang,^{1,61} W. X. Fang,¹ Y. Fang,¹ R. Farinelli,^{29a} L. Fava,^{72b,72c} F. Feldbauer,⁴ G. Felici,^{28a} C. Q. Feng,^{69,56} J. H. Feng,⁵⁷ K. Fischer,⁶⁷ M. Fritsch,⁴ C. Fritsch,⁶⁶ C. D. Fu,¹ Y. W. Fu,¹ H. Gao,⁶¹ Y. N. Gao,^{45,g} Yang Gao,^{69,56} S. Garbolino,^{72c} I. Garzia,^{29a,29b} P. T. Ge,⁷⁴ Z. W. Ge,⁴¹ C. Geng,⁵⁷ E. M. Gersabeck,⁶⁵ A. Gilman,⁶⁷ K. Goetzen,¹⁴ L. Gong,³⁹

W. X. Gong,^{1,56} W. Gradl,³⁴ S. Gramigna,^{29a,29b} M. Greco,^{72a,72c} M. H. Gu,^{1,56} Y. T. Gu,¹⁶ C. Y. Guan,^{1,61} Z. L. Guan,²² A. Q. Guo,^{30,61} L. B. Guo,⁴⁰ R. P. Guo,⁴⁷ Y. P. Guo,^{12,f} A. Guskov,^{35,a} X. T. H.,^{1,61} W. Y. Han,³⁸ X. Q. Hao,²⁰ F. A. Harris,⁶³ K. K. He,⁵³ K. L. He,^{1,61} F. H. Heinsius,⁴ C. H. Heinz,³⁴ Y. K. Heng,^{1,56,61} C. Herold,⁵⁸ T. Holtmann,⁴ P. C. Hong,^{12,f} G. Y. Hou,^{1,61} Y. R. Hou,⁶¹ Z. L. Hou,¹ H. M. Hu,^{1,61} J. F. Hu,^{54,i} T. Hu,^{1,56,61} Y. Hu,¹ G. S. Huang,^{69,56} K. X. Huang,⁵⁷ L. Q. Huang,^{30,61} X. T. Huang,⁴⁸ Y. P. Huang,¹ T. Hussain,⁷¹ N. Hüsken,^{27,34} W. Imoehl,²⁷ M. Irshad,^{69,56} J. Jackson,²⁷ S. Jaeger,⁴ S. Janchiv,³¹ J. H. Jeong,¹⁰ Q. Ji,¹ Q. P. Ji,²⁰ X. B. Ji,^{1,61} X. L. Ji,^{1,56} Y. Y. Ji,⁴⁸ Z. K. Jia,^{69,56} P. C. Jiang,^{45,g} S. S. Jiang,³⁸ T. J. Jiang,¹⁷ X. S. Jiang,^{1,56,61} Y. Jiang,⁶¹ J. B. Jiao,⁴⁸ Z. Jiao,²³ S. Jin,⁴¹ Y. Jin,⁶⁴ M. Q. Jing,^{1,61} T. Johansson,⁷³ X. K.,¹ S. Kabana,³² N. Kalantar-Nayestanaki,⁶² X. L. Kang,⁹ X. S. Kang,³⁹ R. Kappert,⁶² M. Kavatsyuk,⁶² B. C. Ke,⁷⁹ A. Khoukaz,⁶⁶ R. Kiuchi,¹ R. Kliemt,¹⁴ L. Koch,³⁶ O. B. Kolcu,^{60a} B. Kopf,⁴ M. Kuessner,⁴ A. Kupsc,^{43,73} W. Kühn,³⁶ J. J. Lane,⁶⁵ J. S. Lange,³⁶ P. Larin,¹⁹ A. Lavania,²⁶ L. Lavezzi,^{72a,72c} T. T. Lei,^{69,k} Z. H. Lei,^{69,56} H. Leithoff,³⁴ M. Lellmann,³⁴ T. Lenz,³⁴ C. Li,⁴⁶ C. Li,⁴² C. H. Li,³⁸ Cheng Li,^{69,56} D. M. Li,⁷⁹ F. Li,^{1,56} G. Li,¹ H. Li,^{69,56} H. B. Li,^{1,61} H. J. Li,²⁰ H. N. Li,^{54,i} Hui Li,⁴² J. R. Li,⁵⁹ J. S. Li,⁵⁷ J. W. Li,⁴⁸ Ke Li,¹ L. J. Li,^{1,61} L. K. Li,¹ Lei Li,³ M. H. Li,⁴² P. R. Li,^{37,j,k} S. X. Li,¹² T. Li,⁴⁸ W. D. Li,^{1,61} W. G. Li,¹ X. H. Li,^{69,56} X. L. Li,⁴⁸ Xiaoyu Li,^{1,61} Y. G. Li,^{45,g} Z. J. Li,⁵⁷ Z. X. Li,¹⁶ Z. Y. Li,⁵⁷ C. Liang,⁴¹ H. Liang,³³ H. Liang,^{69,56} H. Liang,^{1,61} Y. F. Liang,⁵² Y. T. Liang,^{30,61} G. R. Liao,¹⁵ L. Z. Liao,⁴⁸ J. Libby,²⁶ A. Limphirat,⁵⁸ D. X. Lin,^{30,61} T. Lin,¹ B. X. Liu,⁷⁴ B. J. Liu,¹ C. Liu,³³ C. X. Liu,¹ D. Liu,^{19,69} F. H. Liu,⁵¹ Fang Liu,¹ Feng Liu,⁶ G. M. Liu,^{54,i} H. Liu,^{37,j,k} H. B. Liu,¹⁶ H. M. Liu,^{1,61} Huanhuan Liu,¹ Huihui Liu,²¹ J. B. Liu,^{69,56} J. L. Liu,⁷⁰ J. Y. Liu,^{1,61} K. Liu,¹ K. Y. Liu,³⁹ Ke Liu,²² L. Liu,^{69,56} L. C. Liu,⁴² Lu Liu,⁴² M. H. Liu,^{12,f} P. L. Liu,¹ Q. Liu,⁶¹ S. B. Liu,^{69,56} T. Liu,^{12,f} W. K. Liu,⁴² W. M. Liu,^{69,56} X. Liu,^{37,j,k} Y. Liu,^{37,j,k} Y. B. Liu,⁴² Z. A. Liu,^{1,56,61} Z. Q. Liu,⁴⁸ X. C. Lou,^{1,56,61} F. X. Lu,⁵⁷ H. J. Lu,²³ J. G. Lu,^{1,56} X. L. Lu,¹ Y. Lu,⁷ Y. P. Lu,^{1,56} Z. H. Lu,^{1,61} C. L. Luo,⁴⁰ M. X. Luo,⁷⁸ T. Luo,^{12,f} X. L. Luo,^{1,56} X. R. Lyu,⁶¹ Y. F. Lyu,⁴² F. C. Ma,³⁹ H. L. Ma,¹ J. L. Ma,^{1,61} L. L. Ma,⁴⁸ M. M. Ma,^{1,61} Q. M. Ma,¹ R. Q. Ma,^{1,61} R. T. Ma,⁶¹ X. Y. Ma,^{1,56} Y. Ma,^{45,g} F. E. Maas,¹⁹ M. Maggiora,^{72a,72c} S. Maldaner,⁴ S. Malde,⁶⁷ A. Mangoni,^{28b} Y. J. Mao,^{45,g} Z. P. Mao,¹ S. Marcello,^{72a,72c} Z. X. Meng,⁶⁴ J. G. Messchendorp,^{14,62} G. Mezzadri,^{29a} H. Miao,^{1,61} T. J. Min,⁴¹ R. E. Mitchell,²⁷ X. H. Mo,^{1,56,61} N. Yu. Muchnoi,^{13,b} Y. Nefedov,³⁵ F. Nerling,^{19,d} I. B. Nikolaev,^{13,b} Z. Ning,^{1,56} S. Nisar,^{11,1} Y. Niu,⁴⁸ S. L. Olsen,⁶¹ Q. Ouyang,^{1,56,61} S. Pacetti,^{28b,28c} X. Pan,⁵³ Y. Pan,⁵⁵ A. Pathak,³³ Y. P. Pei,^{69,56} M. Pelizaeus,⁴ H. P. Peng,^{69,56} K. Peters,^{14,d} J. L. Ping,⁴⁰ R. G. Ping,^{1,61} S. Plura,³⁴ S. Pogodin,³⁵ V. Prasad,³² F. Z. Qi,¹ H. Qi,^{69,56} H. R. Qi,⁵⁹ M. Qi,⁴¹ T. Y. Qi,^{12,f} S. Qian,^{1,56} W. B. Qian,⁶¹ C. F. Qiao,⁶¹ J. J. Qin,⁷⁰ L. Q. Qin,¹⁵ X. P. Qin,^{12,f} X. S. Qin,⁴⁸ Z. H. Qin,^{1,56} J. F. Qiu,¹ S. Q. Qu,⁵⁹ C. F. Redmer,³⁴ K. J. Ren,³⁸ A. Rivetti,^{72c} V. Rodin,⁶² M. Rolo,^{72c} G. Rong,^{1,61} Ch. Rosner,¹⁹ S. N. Ruan,⁴² A. Sarantsev,^{35,c} Y. Schelhaas,³⁴ K. Schoenning,⁷³ M. Scodeggio,^{29a,29b} K. Y. Shan,^{12,f} W. Shan,²⁴ X. Y. Shan,^{69,56} J. F. Shangguan,⁵³ L. G. Shao,^{1,61} M. Shao,^{69,56} C. P. Shen,^{12,f} H. F. Shen,^{1,61} W. H. Shen,⁶¹ X. Y. Shen,^{1,61} B. A. Shi,⁶¹ H. C. Shi,^{69,56} J. Y. Shi,¹ Q. Q. Shi,⁵³ R. S. Shi,^{1,61} X. Shi,^{1,56} J. J. Song,²⁰ T. Z. Song,⁵⁷ W. M. Song,^{33,1} Y. X. Song,^{45,g} S. Sosio,^{72a,72c} S. Spataro,^{72a,72c} F. Stieler,³⁴ Y. J. Su,⁶¹ G. B. Sun,⁷⁴ G. X. Sun,¹ H. Sun,⁶¹ H. K. Sun,¹ J. F. Sun,²⁰ K. Sun,⁵⁹ L. Sun,⁷⁴ S. S. Sun,^{1,61} T. Sun,^{1,61} W. Y. Sun,³³ Y. Sun,⁹ Y. J. Sun,^{69,56} Y. Z. Sun,¹ Z. T. Sun,⁴⁸ Y. X. Tan,^{69,56} C. J. Tang,⁵² G. Y. Tang,¹ J. Tang,⁵⁷ Y. A. Tang,⁷⁴ L. Y. Tao,⁷⁰ Q. T. Tao,^{25,h} M. Tat,⁶⁷ J. X. Teng,^{69,56} V. Thoren,⁷³ W. H. Tian,⁵⁰ W. H. Tian,⁵⁷ Y. Tian,^{30,61} Z. F. Tian,⁷⁴ I. Uman,^{60b} B. Wang,^{69,56} B. Wang,¹ B. L. Wang,⁶¹ C. W. Wang,⁴¹ D. Y. Wang,^{45,g} F. Wang,⁷⁰ H. J. Wang,^{37,j,k} H. P. Wang,^{1,61} K. Wang,^{1,56} L. L. Wang,¹ M. Wang,⁴⁸ Meng Wang,^{1,61} S. Wang,^{12,f} T. Wang,^{12,f} T. J. Wang,⁴² W. Wang,⁵⁷ W. Wang,⁷⁰ W. H. Wang,⁷⁴ W. P. Wang,^{69,56} X. Wang,^{45,g} X. F. Wang,^{37,j,k} X. J. Wang,³⁸ X. L. Wang,^{12,f} Y. Wang,⁵⁹ Y. D. Wang,⁴⁴ Y. F. Wang,^{1,56,61} Y. H. Wang,⁴⁶ Y. N. Wang,⁴⁴ Y. Q. Wang,¹ Yaqian Wang,^{18,1} Yi Wang,⁵⁹ Z. Wang,^{1,56} Z. L. Wang,⁷⁰ Z. Y. Wang,^{1,61} Ziyi Wang,⁶¹ D. Wei,⁶⁸ D. H. Wei,¹⁵ F. Weidner,⁶⁶ S. P. Wen,¹ C. W. Wenzel,⁴ U. Wiedner,⁴ G. Wilkinson,⁶⁷ M. Wolke,⁷³ L. Wollenberg,⁴ C. Wu,³⁸ J. F. Wu,^{1,61} L. H. Wu,¹ L. J. Wu,^{1,61} X. Wu,^{12,f} X. H. Wu,³³ Y. Wu,⁶⁹ Y. J. Wu,³⁰ Z. Wu,^{1,56} L. Xia,^{69,56} X. M. Xian,³⁸ T. Xiang,^{45,g} D. Xiao,^{37,j,k} G. Y. Xiao,⁴¹ H. Xiao,^{12,f} S. Y. Xiao,¹ Y. L. Xiao,^{12,f} Z. J. Xiao,⁴⁰ C. Xie,⁴¹ X. H. Xie,^{45,g} Y. Xie,⁴⁸ Y. G. Xie,^{1,56} Y. H. Xie,⁶ Z. P. Xie,^{69,56} T. Y. Xing,^{1,61} C. F. Xu,^{1,61} C. J. Xu,⁵⁷ G. F. Xu,¹ H. Y. Xu,⁶⁴ Q. J. Xu,¹⁷ W. L. Xu,⁶⁴ X. P. Xu,⁵³ Y. C. Xu,⁷⁶ Z. P. Xu,⁴¹ F. Yan,^{12,f} L. Yan,^{12,f} W. B. Yan,^{69,56} W. C. Yan,⁷⁹ X. Q. Yan,¹ H. J. Yang,^{49,e} H. L. Yang,³³ H. X. Yang,¹ Tao Yang,¹ Y. Yang,^{12,f} Y. F. Yang,⁴² Y. X. Yang,^{1,61} Yifan Yang,^{1,61} M. Ye,^{1,56} M. H. Ye,⁸ J. H. Yin,¹ Z. Y. You,⁵⁷ B. X. Yu,^{1,56,61} C. X. Yu,⁴² G. Yu,^{1,61} T. Yu,⁷⁰ X. D. Yu,^{45,g} C. Z. Yuan,^{1,61} L. Yuan,² S. C. Yuan,¹ X. Q. Yuan,¹ Y. Yuan,^{1,61} Z. Y. Yuan,⁵⁷ C. X. Yue,³⁸ A. A. Zafar,⁷¹ F. R. Zeng,⁴⁸ X. Zeng,^{12,f} Y. Zeng,^{25,h} X. Y. Zhai,³³ Y. H. Zhan,⁵⁷ A. Q. Zhang,^{1,61} B. L. Zhang,^{1,61} B. X. Zhang,¹ D. H. Zhang,⁴² G. Y. Zhang,²⁰ H. Zhang,⁶⁹ H. H. Zhang,³³ H. H. Zhang,⁵⁷ H. Q. Zhang,^{1,56,61} H. Y. Zhang,^{1,56} J. J. Zhang,⁵⁰ J. L. Zhang,⁷⁵ J. Q. Zhang,⁴⁰ J. W. Zhang,^{1,56,61} J. X. Zhang,^{37,j,k} J. Y. Zhang,¹ J. Z. Zhang,^{1,61} Jiawei Zhang,^{1,61} L. M. Zhang,⁵⁹ L. Q. Zhang,⁵⁷ Lei Zhang,⁴¹ P. Zhang,¹ Q. Y. Zhang,^{38,79}

Shuihan Zhang,^{1,61} Shulei Zhang,^{25,h} X. D. Zhang,⁴⁴ X. M. Zhang,¹ X. Y. Zhang,⁵³ X. Y. Zhang,⁴⁸ Y. Zhang,⁶⁷ Y. T. Zhang,⁷⁹
 Y. H. Zhang,^{1,56} Yan Zhang,^{69,56} Yao Zhang,¹ Z. H. Zhang,¹ Z. L. Zhang,³³ Z. Y. Zhang,⁴² Z. Y. Zhang,⁷⁴ G. Zhao,¹ J. Zhao,³⁸
 J. Y. Zhao,^{1,61} J. Z. Zhao,^{1,56} Lei Zhao,^{69,56} Ling Zhao,¹ M. G. Zhao,⁴² S. J. Zhao,⁷⁹ Y. B. Zhao,^{1,56} Y. X. Zhao,^{30,61}
 Z. G. Zhao,^{69,56} A. Zhemchugov,^{35,a} B. Zheng,⁷⁰ J. P. Zheng,^{1,56} W. J. Zheng,^{1,61} Y. H. Zheng,⁶¹ B. Zhong,⁴⁰ X. Zhong,⁵⁷
 H. Zhou,⁴⁸ L. P. Zhou,^{1,61} X. Zhou,⁷⁴ X. R. Zhou,^{69,56} X. Y. Zhou,³⁸ Y. Z. Zhou,^{12,f} J. Zhu,⁴² K. Zhu,¹ K. J. Zhu,^{1,56,61}
 L. Zhu,³³ L. X. Zhu,⁶¹ S. H. Zhu,⁶⁸ S. Q. Zhu,⁴¹ T. J. Zhu,^{12,f} W. J. Zhu,^{12,f} Y. C. Zhu,^{69,56}
 Z. A. Zhu,^{1,61} J. H. Zou,¹ and J. Zu^{69,56}

(BESIII Collaboration)

¹*Institute of High Energy Physics, Beijing 100049, People's Republic of China*

²*Beihang University, Beijing 100191, People's Republic of China*

³*Beijing Institute of Petrochemical Technology, Beijing 102617, People's Republic of China*

⁴*Bochum Ruhr-University, D-44780 Bochum, Germany*

⁵*Carnegie Mellon University, Pittsburgh, Pennsylvania 15213, USA*

⁶*Central China Normal University, Wuhan 430079, People's Republic of China*

⁷*Central South University, Changsha 410083, People's Republic of China*

⁸*China Center of Advanced Science and Technology, Beijing 100190, People's Republic of China*

⁹*China University of Geosciences, Wuhan 430074, People's Republic of China*

¹⁰*Chung-Ang University, Seoul 06974, Republic of Korea*

¹¹*COMSATS University Islamabad, Lahore Campus, Defence Road, Off Raiwind Road,
54000 Lahore, Pakistan*

¹²*Fudan University, Shanghai 200433, People's Republic of China*

¹³*G.I. Budker Institute of Nuclear Physics SB RAS (BINP), Novosibirsk 630090, Russia*

¹⁴*GSI Helmholtzcentre for Heavy Ion Research GmbH, D-64291 Darmstadt, Germany*

¹⁵*Guangxi Normal University, Guilin 541004, People's Republic of China*

¹⁶*Guangxi University, Nanning 530004, People's Republic of China*

¹⁷*Hangzhou Normal University, Hangzhou 310036, People's Republic of China*

¹⁸*Hebei University, Baoding 071002, People's Republic of China*

¹⁹*Helmholtz Institute Mainz, Staudinger Weg 18, D-55099 Mainz, Germany*

²⁰*Henan Normal University, Xinxiang 453007, People's Republic of China*

²¹*Henan University of Science and Technology, Luoyang 471003, People's Republic of China*

²²*Henan University of Technology, Zhengzhou 450001, People's Republic of China*

²³*Huangshan College, Huangshan 245000, People's Republic of China*

²⁴*Hunan Normal University, Changsha 410081, People's Republic of China*

²⁵*Hunan University, Changsha 410082, People's Republic of China*

²⁶*Indian Institute of Technology Madras, Chennai 600036, India*

²⁷*Indiana University, Bloomington, Indiana 47405, USA*

^{28a}*INFN Laboratori Nazionali di Frascati, I-00044 Frascati, Italy*

^{28b}*INFN Sezione di Perugia, I-06100 Perugia, Italy*

^{28c}*University of Perugia, I-06100 Perugia, Italy*

^{29a}*INFN Sezione di Ferrara, I-44122 Ferrara, Italy*

^{29b}*University of Ferrara, I-44122 Ferrara, Italy*

³⁰*Institute of Modern Physics, Lanzhou 730000, People's Republic of China*

³¹*Institute of Physics and Technology, Peace Avenue 54B, Ulaanbaatar 13330, Mongolia*

³²*Instituto de Alta Investigación, Universidad de Tarapacá, Casilla 7D, Arica, Chile*

³³*Jilin University, Changchun 130012, People's Republic of China*

³⁴*Johannes Gutenberg University of Mainz, Johann-Joachim-Becher-Weg 45, D-55099 Mainz, Germany*

³⁵*Joint Institute for Nuclear Research, 141980 Dubna, Moscow region, Russia*

³⁶*Justus-Liebig-Universitaet Giessen, II. Physikalisches Institut, Heinrich-Buff-Ring 16,
D-35392 Giessen, Germany*

³⁷*Lanzhou University, Lanzhou 730000, People's Republic of China*

³⁸*Liaoning Normal University, Dalian 116029, People's Republic of China*

³⁹*Liaoning University, Shenyang 110036, People's Republic of China*

⁴⁰*Nanjing Normal University, Nanjing 210023, People's Republic of China*

⁴¹*Nanjing University, Nanjing 210093, People's Republic of China*

⁴²*Nankai University, Tianjin 300071, People's Republic of China*

⁴³*National Centre for Nuclear Research, Warsaw 02-093, Poland*

- ⁴⁴North China Electric Power University, Beijing 102206, People's Republic of China
⁴⁵Peking University, Beijing 100871, People's Republic of China
⁴⁶Qufu Normal University, Qufu 273165, People's Republic of China
⁴⁷Shandong Normal University, Jinan 250014, People's Republic of China
⁴⁸Shandong University, Jinan 250100, People's Republic of China
⁴⁹Shanghai Jiao Tong University, Shanghai 200240, People's Republic of China
⁵⁰Shanxi Normal University, Linfen 041004, People's Republic of China
⁵¹Shanxi University, Taiyuan 030006, People's Republic of China
⁵²Sichuan University, Chengdu 610064, People's Republic of China
⁵³Soochow University, Suzhou 215006, People's Republic of China
⁵⁴South China Normal University, Guangzhou 510006, People's Republic of China
⁵⁵Southeast University, Nanjing 211100, People's Republic of China
⁵⁶State Key Laboratory of Particle Detection and Electronics, Beijing 100049, Hefei 230026, People's Republic of China
⁵⁷Sun Yat-Sen University, Guangzhou 510275, People's Republic of China
⁵⁸Suranaree University of Technology, University Avenue 111, Nakhon Ratchasima 30000, Thailand
⁵⁹Tsinghua University, Beijing 100084, People's Republic of China
^{60a}Turkish Accelerator Center Particle Factory Group, Istinye University, 34010 Istanbul, Turkey
^{60b}Near East University, Nicosia, North Cyprus 99138, Mersin 10, Turkey
⁶¹University of Chinese Academy of Sciences, Beijing 100049, People's Republic of China
⁶²University of Groningen, NL-9747 AA Groningen, The Netherlands
⁶³University of Hawaii, Honolulu, Hawaii 96822, USA
⁶⁴University of Jinan, Jinan 250022, People's Republic of China
⁶⁵University of Manchester, Oxford Road, Manchester M13 9PL, United Kingdom
⁶⁶University of Muenster, Wilhelm-Klemm-Strasse 9, 48149 Muenster, Germany
⁶⁷University of Oxford, Keble Road, Oxford OX13RH, United Kingdom
⁶⁸University of Science and Technology Liaoning, Anshan 114051, People's Republic of China
⁶⁹University of Science and Technology of China, Hefei 230026, People's Republic of China
⁷⁰University of South China, Hengyang 421001, People's Republic of China
⁷¹University of the Punjab, Lahore-54590, Pakistan
^{72a}University of Turin, I-10125 Turin, Italy
^{72b}University of Eastern Piedmont, I-15121 Alessandria, Italy
^{72c}INFN, I-10125 Turin, Italy
⁷³Uppsala University, Box 516, SE-75120 Uppsala, Sweden
⁷⁴Wuhan University, Wuhan 430072, People's Republic of China
⁷⁵Xinyang Normal University, Xinyang 464000, People's Republic of China
⁷⁶Yantai University, Yantai 264005, People's Republic of China
⁷⁷Yunnan University, Kunming 650500, People's Republic of China
⁷⁸Zhejiang University, Hangzhou 310027, People's Republic of China
⁷⁹Zhengzhou University, Zhengzhou 450001, People's Republic of China

^aAlso at the Moscow Institute of Physics and Technology, Moscow 141700, Russia.

^bAlso at the Novosibirsk State University, Novosibirsk 630090, Russia.

^cAlso at the NRC "Kurchatov Institute", PNPI, 188300 Gatchina, Russia.

^dAlso at Goethe University Frankfurt, 60323 Frankfurt am Main, Germany.

^eAlso at Key Laboratory for Particle Physics, Astrophysics and Cosmology, Ministry of Education; Shanghai Key Laboratory for Particle Physics and Cosmology; Institute of Nuclear and Particle Physics, Shanghai 200240, People's Republic of China.

^fAlso at Key Laboratory of Nuclear Physics and Ion-beam Application (MOE) and Institute of Modern Physics, Fudan University, Shanghai 200443, People's Republic of China.

^gAlso at State Key Laboratory of Nuclear Physics and Technology, Peking University, Beijing 100871, People's Republic of China.

^hAlso at School of Physics and Electronics, Hunan University, Changsha 410082, China.

ⁱAlso at Guangdong Provincial Key Laboratory of Nuclear Science, Institute of Quantum Matter, South China Normal University, Guangzhou 510006, China.

^jAlso at Frontiers Science Center for Rare Isotopes, Lanzhou University, Lanzhou 730000, People's Republic of China.

^kAlso at Lanzhou Center for Theoretical Physics, Lanzhou University, Lanzhou 730000, People's Republic of China.

^lAlso at the Department of Mathematical Sciences, IBA, Krachi, Pakistan.